Exploring the properties of the M31 halo globular cluster system

A. P. Huxor,[1]⋆† A. M. N. Ferguson,[1] N. R. Tanvir,[2] M. J. Irwin,[3] A. D. Mackey,[1]‡
R. A. Ibata,[4] T. Bridges,[5] S. C. Chapman[3] and G. F. Lewis[6]

[1]*Institute for Astronomy, University of Edinburgh, Royal Observatory, Blackford Hill, Edinburgh EH9 3HJ*
[2]*Department of Physics and Astronomy, University of Leicester, University Road, Leicester LE1 7RH*
[3]*Institute of Astronomy, Madingley Road, Cambridge CB3 0HA*
[4]*Observatoire de Strasbourg, 11, rue de l'Universite, F-67000 Strasbourg, France*
[5]*Department of Physics, Queen's University, Kingston, Ontario K7M 3N6, Canada*
[6]*Sydney Institute for Astronomy, School of Physics, A29, University of Sydney, NSW 2006, Australia*

ABSTRACT

Following on from our discovery of a significant population of M31 outer halo globular clusters (GCs), and updates to the Revised Bologna Catalogue of M31 GCs, we investigate the GC system of M31 out to an unprecedented radius ($\approx$120 kpc). We derive various ensemble properties, including the magnitude, colour and metallicity distributions, as well as the GC number density profile. One of our most significant findings is evidence for a flattening in the radial GC number density profile in the outer halo. Intriguingly, this occurs at a galactocentric radius of $\sim 2°$ ($\sim$30 kpc) which is the radius at which the underlying stellar halo surface density has also been shown to flatten. The GCs which lie beyond this radius are remarkably uniform in terms of their blue $(V-I)_0$ colours, consistent with them belonging to an ancient population with little to no metallicity gradient. Structural parameters are also derived for a sample of 13 newly discovered extended clusters (ECs), and we find the lowest luminosity ECs have magnitudes and sizes similar to Palomar-type GCs in the Milky Way halo. We argue that our findings provide strong support for a scenario in which a significant fraction of the outer halo GC population of M31 has been accreted.

Key words: galaxies: evolution – galaxies: formation – galaxies: haloes – galaxies: individual: M31 – galaxies: interactions – galaxies: star clusters: general.

1 INTRODUCTION

The properties of globular cluster (GC) systems provide valuable probes of the formation and evolution of their host galaxies (e.g. West et al. 2004; Brodie & Strader 2006). It is commonly believed that GCs form in major star-forming episodes that accompany galaxy formation, as well as in subsequent merger events (e.g. Zepf & Ashman 1993). Furthermore, the native GC population of a galaxy is expected to be augmented through mergers with and accretions of smaller systems, each of which will bring its own retinue of GCs into the final galaxy. As a result, the GC population of a galaxy will reflect both the amount of mass formed *in situ*, as well as that which has been accreted.

As GCs are (mostly) luminous and compact, they can be readily observed in galaxies up to a few hundred Mpc distance. Nevertheless, the GC systems of Local Group galaxies remain of central importance as they allow the most detailed study of the properties of GC populations and how they correlate with the formation history of their host galaxies. This is possible as their proximity permits studies of resolved field and cluster stellar populations through their colour–magnitude diagrams (CMDs; e.g. Mackey et al. 2006) and spectroscopy (e.g. Barmby et al. 2000).

The study of the Galactic GC system by Searle & Zinn (1978) proved crucial for understanding the history of our own Milky Way (MW). Their analysis of GC metallicities within the halo led them to conclude that many of these objects must have formed within protogalactic fragments that fell into the Galaxy after the collapse of the central regions had been completed. This scenario was in stark contrast to the monolithic slow collapse picture earlier proposed by Eggen, Lynden-Bell & Sandage (1962). One of the main distinguishing characteristics of the two models was the halo

⋆E-mail: Avon.Huxor@bristol.ac.uk
†Present address: H. H. Wills Physics Laboratory, Tyndall Avenue, Bristol BS8 1TL.
‡Present address: Research School of Astronomy & Astrophysics, Australian National University, Mt Stromlo Observatory, Cotter Road, Weston Creek, ACT 2611, Australia.

metallicity gradient; the latter scenario predicted a radial gradient with clusters nearer to the centre being more metal rich, as they were formed somewhat later in the collapse, while the former predicted a spread in metallicities at all radii but no significant radial variation. Modern theories of galaxy assembly are based on hierarchical structure formation with galaxies forming inside dark matter haloes (e.g. White & Frenk 1991). Although this model bears some similarities to the scenario proposed by Searle & Zinn, there are also several differences. In particular, it has been shown that build-up via accretion can sometimes lead to halo metallicity gradients since massive satellites, which are normally more metal rich, sink further into the potential well of the host than do low-mass objects (e.g. De Lucia & Helmi 2008; Font et al. 2008). Thus, while the lack of a halo metallicity gradient argues against slow pressure-supported collapse, the existence of one could be consistent with both that scenario as well as accretion.

The GC system of M31 has also been studied intensively in order to search for clues about how that system formed and evolved (e.g. Crampton et al. 1985; Elson & Walterbos 1988; Huchra, Brodie & Kent 1991; Barmby et al. 2000; Perrett et al. 2002; Fan et al. 2008). Since M31 is similar to the MW in many respects, it may be expected to have experienced a similar assembly history. Early work suggested a mild gradient in the metallicity of the M31 GC system (e.g. Sharov 1988; Huchra et al. 1991; Barmby et al. 2000). Perrett et al. (2002) and Fan et al. (2008) found that this result is primarily driven by a metallicity gradient in the metal-poor GCs alone, while Perrett et al. (2002) noted that the slope of the gradient may flatten beyond a projected radius of ∼14 kpc.

In addition to the metallicity gradient, another key property of a GC system is the radial profile – the areal number density of GCs as a function of distance from the centre of the host galaxy. Radial GC profiles have traditionally been represented with either a power law (i.e. R^{-n}) or a de Vaucouleurs law (i.e. $R^{1/4}$ law), with a flattening of the profile at small radii, and a gradual steepening in the outer regions (Brodie & Strader 2006). The most recently published GC surface density profile in M31 is that of Battistini et al. (1993), who experimented with a variety of fitting formulae. Using a sample which extended to a radius of ∼30 kpc, they noted that their data were consistent with a steepening in the outer regions, earlier found by Racine (1991), if one uses the general power – or $R^{1/4}$ laws (although this is not the case if they employ an $R^{1/1.6}$ law). They argued that this steepening was unlikely to be due to incompleteness in their sample at large radius, although the possibility could not be completely excluded.

A major limitation of all previous studies of the ensemble properties of the M31 GC system has been the restricted radial range of the samples. These studies have generally employed samples extending to no more than ∼25 kpc, while analogous studies of the MW GC system have extended to beyond 100 kpc. In the last decade, vast amounts of new imaging have been obtained of the outer regions of M31, revealing that both field stars and GCs extend to radii of well over 100 kpc (e.g. Ferguson et al. 2002; Ibata et al. 2007; Huxor et al. 2008; McConnachie et al. 2009; Mackey et al. 2010a). It is therefore timely to revisit the properties of the M31 GC system in light of these new data sets. In Section 2, we discuss the sample used for our study which consists of the Revised Bologna Catalogue (RBC) and new GCs presented in Huxor et al. (2008, hereafter Paper I). In Section 3, we discuss radially dependent properties of the M31 GC system using a baseline that extends over 100 kpc. In Section 4, we discuss properties of extended star clusters in M31's outer halo. Section 5 discusses our findings in the context of the assembly history of M31.

2 THE SAMPLE

The sample of GCs used in this study is taken from version V3.5[1] of the RBC, which was released in 2008 March.[2] A full description of the RBC can be found in Galleti et al. (2004) with updates in Galleti et al. (2006) and Galleti et al. (2007). It contains 1983 entries, including 509 confirmed GCs, 13 confirmed extended clusters (ECs) and 1049 'candidate clusters'. This version of the RBC includes 103 confirmed objects reported by Kim et al. (2007) although subsequent work has shown that many of these objects have been improperly classified (Caldwell et al. 2009; Peacock et al. 2010). This has only a minor impact on the results presented here as the Kim et al. objects all lie within a projected radius of 18 kpc (90 per cent within 10 kpc) from the centre of M31, while our main focus in this paper is on the halo regions beyond 20 kpc. The RBC V3.5 also includes the 40 new outer halo clusters found by our group and reported in Paper I. In brief, these latter objects were discovered in more than 80 deg² of imaging survey data taken with the Wide Field Camera on the Isaac Newton Telescope (INT) and MegaCam on the Canada–France–Hawaii Telescope (CFHT; see Ferguson et al. 2002, and Ibata et al. 2007, for details of the surveys). Thanks to the quality of the seeing conditions and the proximity of M31 to us, the clusters could all be identified as marginally or fully resolved stellar concentrations. The new clusters we discovered increased the total number of confirmed GCs in M31 known at the time of publication by a modest amount (∼10 per cent), but the number of confirmed GCs known beyond 1° (≈14 kpc) increased by more than 75 per cent.

For the main sample used in our analysis, we select clusters in the RBC V3.5 that have a *Global classification flag* (f) equal to 1 or 8 corresponding to 'confirmed' GCs and ECs, respectively. Although the RBC uses this flag to distinguish between ECs and GCs, studies to date suggest M31 ECs have the same ancient stellar content as GCs (Mackey et al. 2006), hence we consider them together in the present work. The very remote GC found by Martin et al. (2006) and recently studied in detail by Mackey et al. (2010a) is included in the sample for most of the analysis but not for the GC surface density profile as it lies in an area of the CFHT/MegaCam survey for which full results of our GC search have yet to be published. Possible *young* GCs are also excised from our sample by removing those clusters for which the *young cluster* flag (yy) is greater than zero. While M31 appears to have a genuine population of young to intermediate age GCs (e.g. Fusi Pecci et al. 2005; Fan et al. 2006), such a population is absent in the MW. Since our primary interest in this paper is to examine ancient star clusters as probes of galaxy formation, a sample with these young objects removed makes for a more appropriate comparison of the GC systems of both galaxies. The final sample we employ for the bulk of our analysis contains 431 objects, while the sample used for constructing the surface density profile analysis contains 430 objects – removing the Martin et al. (2006) GC as noted above.

The RBC is a compilation of a variety of different data sources and in situations where our own photometry is available from Paper I, this is used in preference to that provided by the RBC for homogeneity. The projected galactocentric radii of the GCs are rederived

---

[1] http://www.bo.astro.it/M31/

[2] While this paper was in preparation, the RBC was updated in 2009 December to V4.0. However, the changes do not affect the results in the present work, as the updates concern a few GCs in the inner region of M31 and added new young clusters. We do not include such young clusters in our sample (see main text).
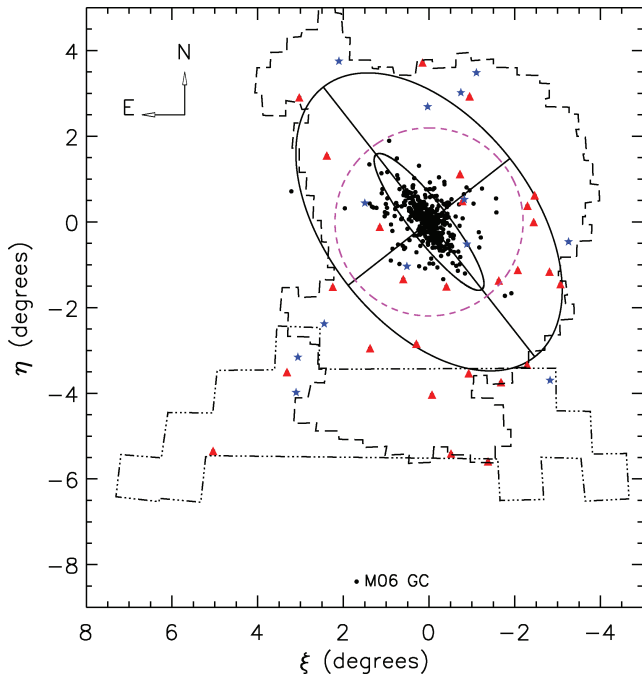
Figure 1. The location of the new GCs (red triangles) and ECs (blue stars) in relation to confirmed RBC GCs that lie in the survey area analysed here (black circles). The limited extent of the known GC population prior to this study can be clearly seen. The dashed line outlines the INT survey area covered, and the dot–dashed line outlines that part of the MegaCam survey employed here. The inner ellipse has a semimajor axis of $2°$ (27 kpc) representing a disc with an inclination of $77°.5$; the optical disc of M31 lies well within this boundary. The outer ellipse denotes a flattened ellipsoid of semimajor axis length $4°$ (55 kpc). The dashed circle lies at a radius of 30 kpc, and shows the region at which the break in the GC surface density profile occurs (see text for details).The outermost GC found by Martin et al. (2006) and discussed by Mackey et al. (2010a) is also shown (M06 GC) and indicates the extent of the currently known M31 halo GC population.

from the equatorial coordinates listed in the RBC using M31 central coordinates of RA = $00^h42^m44^s.3$ and Dec. = $+41°16'09''$ for the centre of M31, taken from NASA/IPAC Extragalactic Database (NED).[3] Fig. 1 shows the spatial distribution of the GCs around M31 in our sample and illustrates the much greater radial extent of our sample compared to those used for previous M31 GC studies.

3 RADIALLY DEPENDENT PROPERTIES OF THE M31 GC SYSTEM

We now proceed to use this sample to derive the basic properties of the M31 GC system out to much larger radius than has been previously done. Wherever possible, we compare the quantities derived with those of the MW GC system for which we use the information listed in the McMaster Catalogue of Milky Way Globular Clusters[4] (Harris 1996). This catalogue lists data for 141 GCs, although not all of them have a full set of derived parameters. The catalogue also does not contain a few very recently discovered MW GCs in the Galactic plane (e.g. Kobulnicky et al. 2005; Kurtev et al. 2008), but since these do not lie at large galactocentric distances, they do not affect our overall results. We do, however, include the two newly discovered GCs found in the outer halo of the MW (Koposov et al.
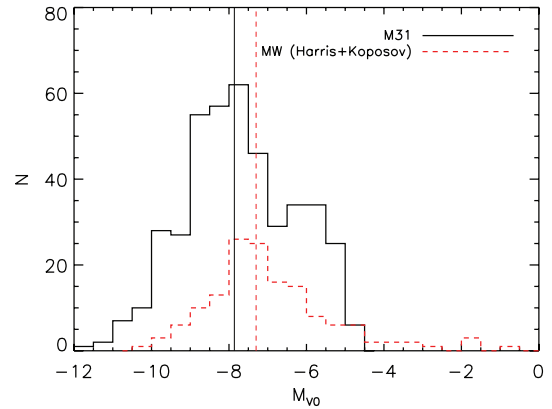
---

[3] http://nedwww.ipac.caltech.edu/

[4] http://physwww.physics.mcmaster.ca/~harris/mwgc.dat

Figure 2. Extinction-corrected absolute *V*-band magnitudes of M31 GCs (black line) in our catalogue, using values of A_V derived from Fan et al. (2010) or Schlegel et al. (1998), depending on availability (see text for details). The red dashed histogram shows the distribution for the MW GCs and includes the Koposov et al. (2007) clusters. Median values for each sample are shown with vertical lines (-7.9 for M31 and -7.3 for the MW).

2007). As there is limited information available for these objects at the present time (only size and *V*-band magnitudes), they can only be used for a subset of the following comparisons. The values of $E(B - V)$ given in the Harris catalogue are used to derive the corrected magnitudes and colours for each MW cluster.

3.1 GC luminosities

The M31 GC luminosity function (GCLF) is shown in Fig. 2. The M31 GC magnitudes have been calculated assuming a distance modulus of 24.47 mag (McConnachie et al. 2005). The magnitudes are corrected for extinction using the $E(B - V)$ values in Fan, de Grijs & Zhou (2010) where available. These values are derived from spectral energy distribution (SED) fits to multiband photometry and give the total line-of-sight extinction including that internal to M31. For those GCs in our sample that were not studied by Fan et al. (2010), we adopt their median value of $E(B - V) = 0.12$, except for the very outer halo GCs ($R_{proj} > 40$ kpc), where we use only Galactic foreground extinction calculated by interpolation of the Schlegel, Finkbeiner & Davis (1998) maps.[5] Previous work on the M31 outer halo GCs (Mackey et al. 2007) gives reddening values consistent with Galactic extinction being the significant component. The MW GCs are overlaid in red.

Although the number of currently confirmed M31 GCs is already approximately three times larger than the number known in the MW, the shapes of their luminosity functions are roughly similar, at least down to an absolute magnitude of $M_{V0} \approx -5$, where completeness issues begin to complicate the M31 sample. Fig. 2 reveals an offset of ~0.6 mag between the peaks of the GCLFs (the medians being -7.9 and -7.3 for M31 and the MW, respectively); however, the magnitude of this offset is very dependent on the assumed extinction for the M31 population. While the Fan et al. (2010) reddening values are the best available as they are derived in a homogeneous manner for a large number of clusters, there are hints that they may overestimate the extinction at high $E(B - V)$ when compared to other methods (see their fig. 7). Indeed, if only Galactic foreground extinction is assumed, there is no discernible offset in the GCLF peaks of M31 and the MW. The M31 GCLF

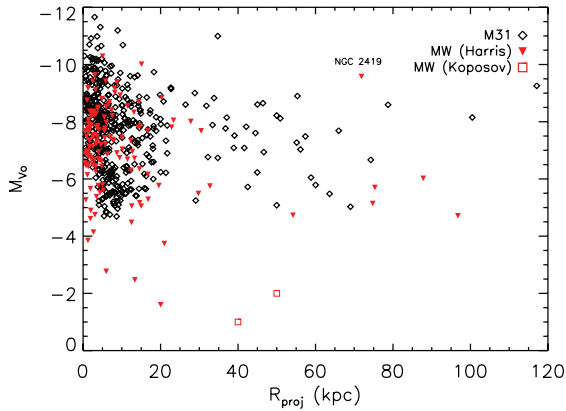[5] http://astro.berkeley.edu/~marc/dust/data/data.html

Figure 3. The radial variation of the extinction-corrected V-band absolute magnitudes for M31 (open diamonds) and the MW (inverted triangles and open squares) GCs, using the same data as Fig. 2. In the case of the MW GCs, the actual distance (R_{gc}) is converted to an 'average projected distance' through $R_{proj} = R_{gc} \times (\pi/4)$. The unusual MW cluster NGC 2419 is labelled.

also exhibits a secondary peak at $M_{V0} \approx -5.5$ that is not seen in the MW population. This peak is present when inner (≤ 20 kpc) and outer (≥ 20 kpc) halo samples are considered separately, suggesting it could be genuine. On the other hand, many of the Kim et al. (2007) clusters have magnitudes around this value, a large fraction of which have questionable classifications (e.g. see the discussion in Peacock et al. 2010). A more detailed comparison of the MW and M31 GCLFs will be carried out at a later date, when uniform photometry and reddenings are available for the entire sample and the completeness and contamination of the M31 catalogue has been more rigorously quantified.

Fig. 3 shows the distribution of absolute magnitudes against projected galactocentric distance for those GCs for which V-band data are available. This includes all but four of the Harris MW catalogue and all but eight of the M31 catalogue. The galactocentric distances for the MW GCs, R_{gc}, are converted to equivalent projected radii using $R_{proj} = \pi/4 \times R_{gc}$. This numerical factor accounts for the ratio of the projected distance to the true distance for an isotropically distributed GC population viewed from a distant random external vantage point.

Fig. 3 reveals that M31 has a population of luminous GCs at large galactocentric distances, a finding previously commented on from studies with smaller data sets (Galleti et al. 2007; Mackey et al. 2007). While these GCs are no more luminous than GCs at smaller radii in M31, they are significantly more luminous than the outer halo GCs in the MW. In the MW, only NGC 2419 has a galactocentric radius larger than $\sim$35 kpc and a luminosity greater than $M_{V0} \lesssim -6.5$, whereas M31 has 21 GCs in this same region of parameter space (even although the sample studied here covers only a quarter of the sky area at these distances). Almost all the outer halo GCs in the MW are 'Palomar-type' clusters with low luminosities and relatively large half-light radii. As both samples are likely to be highly complete in this magnitude range, the difference between the numbers of luminous M31 and MW GCs, a factor of $\sim$20, cannot be solely due to the difference in the overall size of the GC populations (which accounts for only a factor of $\sim$3). It is unclear whether M31 also possesses an excess of faint outer halo GCs compared to the MW since completeness issues currently complicate our analysis below $M_{V0} \approx -5$.
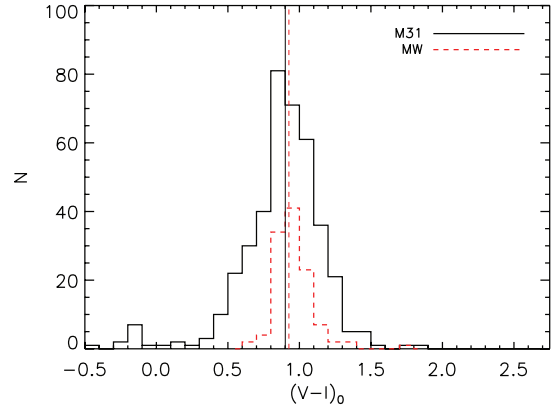
Figure 4. The distribution of $(V - I)_0$ for GCs in M31 (black solid histogram) and the MW (red dashed histogram), where this colour measure is available. Where no I-band data are available for MW GCs, $(V - I)$ colours are derived from $(B - V)$ (see text for details). Median values are shown by the vertical lines. The Koposov et al. (2007) GCs are not included here as no colour information is available for them.

3.2 GC colours and metallicities

Fig. 4 shows histograms of the $(V - I)_0$ colours for the MW and M31 GC samples. Only 96 out of the 141 MW GCs had $(V - I)$ values listed in the Harris data base. As an additional 20 MW GCs had $(B - V)$ data, we fitted the $(V - I)$ colours as a function of $(B - V)$ for those GCs for which both colours were available. This resulted in the relation $(V - I) = 1.23 \times (B - V) + 0.09$ (rms = 0.05), which was used to estimate $(V - I)$ values for those remaining 20 GCs. Fig. 4 shows that the M31 GC system has the same median colour as that of the MW, with the reddening-corrected median $(V - I)_0$ colours being 0.89 and 0.93 mag for M31 and the MW, respectively. This is somewhat at odds with earlier findings that the M31 GC system is, on average, redder than that of the MW (e.g. Huchra et al. 1991) and depends largely on our adopted reddening values from Fan et al. (2010).

When viewed as a function of galactocentric radius (Fig. 5), the mean GC colours in the outer halo are uniformly blue and similar in both systems. We find $(V - I)_0 = 0.87 \pm 0.04$ in M31 for $R \gtrsim 30$ kpc and $(V - I)_0 = 0.92 \pm 0.03$ for $R \gtrsim 15$ kpc in the MW, where errors are the standard error on the mean. The colours are almost identical for $R \gtrsim 45$ kpc, the difference for $R \gtrsim 30$ kpc
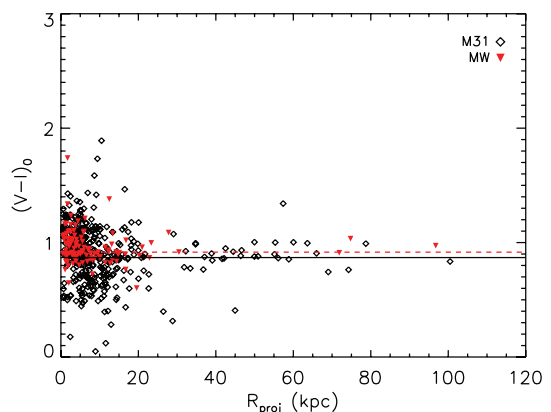

Figure 5. The distribution of $(V - I)_0$ for M31 (open diamonds) and MW (inverted triangles) with galactocentric radius. The data used here are the same as for Fig. 4. The mean colours for the $R_{proj} > 30$ kpc M31 and $R_{proj} > 15$ kpc MW GCs are shown as black and red dashed lines, respectively.
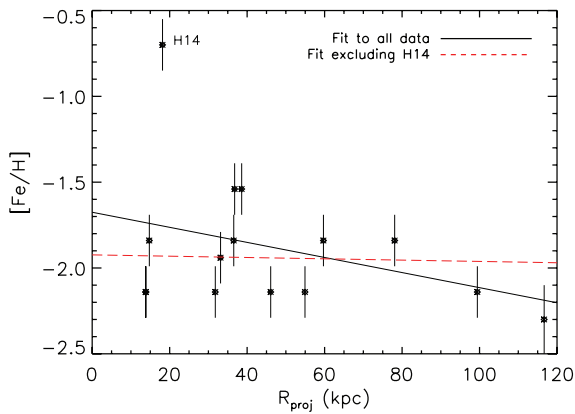
Figure 6. The radial variation of metallicities for those GCs with accurate values in the literature from CMD fitting (Mackey et al. 2006. 2007, 2010a). The solid line is a fit to all the data, and the dashed line is a fit that excludes the outlier, the possibly intermediate-age cluster H14 (Mackey et al. (2007), where is it called GC7. The errors on individual data points are ± 0.15 dex (Mackey et al. 2006, 2007, 2010a).

Figure 7. A log – log plot of the radial number density profile of GCs in M31, with Poisson errors (see text). A broken power law has been fitted, with slopes and errors for each component given in the legend. The inner region extends from the centre of M31 to a projected distance ($R_{\rm proj}$) of ≈ 5 kpc (dotted black line), the intermediate region from $R_{\rm proj} \approx 5$ to ≈ 30 kpc (red dot–dashed line) and the outer region from $R_{\rm proj} \approx 30$ kpc (solid black line). A change in the slope of the profile can be seen at ≈ 5 and 30 kpc. The outer three bins contain 13, 10 and three GCs in the original data which increase to estimated values of ≈ 15, 25 and 27 GCs when the incomplete spatial coverage for each annulus is taken into account.

solely due to the inclusion of the very blue EC HEC1. As small-scale extinction variations are not likely to be a factor in these remote parts, this suggests that intrinsic properties of the outer halo GCs in both systems are very similar. Interestingly, the mean colour of the outer halo GCs in M33 [$(V - I)_0 = 0.88 \pm 0.05$, Huxor et al. 2009] is also very close to the values found in M31 and the MW.

The dispersion in colour of the outer halo GCs in Fig. 5 is relatively small beyond 30 kpc, and there is no evidence of any radial gradient. Since the integrated colour reflects both the age and the metallicity of a GC, further information is required in order to properly interpret the uniformity in the outer halo. For several of the M31 outer halo GCs, we have previously derived metallicities from fitting model isochrones and MW GC fiducials to high-quality CMDs (Mackey et al. 2006, 2007, 2010a). These fits are based exclusively on the red giant and horizontal branch stars. Fig. 6 shows the metallicities derived in this manner for 11 compact and four extended GCs in the M31 halo. A linear least-squares fit to all the data yields a slope of -0.006 ± 0.002 dex kpc^{-1}, indicating a marginal negative gradient. However, there is one clear outlier in the plot – H14 – which was previously flagged by Mackey et al. (2007) as a possible intermediate-age cluster. If true, this would affect the metallicity of the cluster which has been derived assuming a 10 Gyr age. If this object is removed, we obtain the dashed line fit with a mean metallicity of -1.94 ± 0.22 dex and no discernible gradient (-0.003 ± 0.002 dex kpc^{-1}). If we focus only on those GCs which lie beyond 30 kpc, the mean metallicity is effectively the same, given the errors, at -1.95 dex. It thus seems fair to assume that the uniformity in the broad-band colours of the outer halo GCs seen in Fig. 5 reflects a narrow spread in both age and metallicity, with this population being predominantly old and metal poor. For comparison, the average [Fe/H] for the MW sample with $R_{\rm proj} > 15$ kpc is -1.70 ± 0.23 dex (Harris 1996). Our finding of no significant metallicity gradient in the M31 halo GC population is consistent with the study of Alves-Brito et al. (2009), who found the same result from spectroscopic measurements of a small sample of GCs, although we note that there is a discrepancy between the absolute metallicities obtained by these authors and those inferred from our CMD fitting).
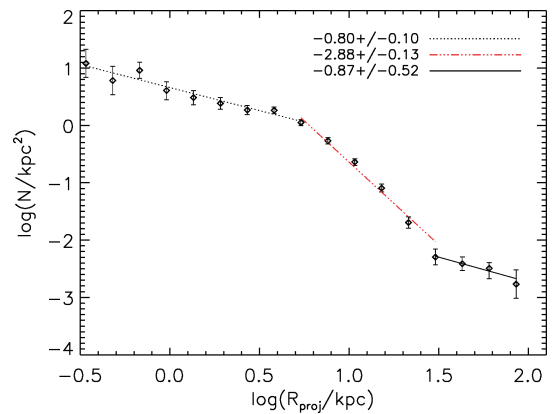
3.3 The radial surface density profile of the M31 GC system

The radial number density profile of the M31 GC system can be calculated in a straightforward fashion once a correction is made for the non-uniform azimuthal coverage of the outer halo surveys from which our GC catalogue has been constructed. Indeed, as can be seen in Fig. 1, the surveys used to identify outer halo GCs extend significantly further in the south-eastern direction than anywhere else. Using knowledge of the field centres and sizes, we determined the proportion of the sky imaged within a specific annulus and hence the correction factor needed to estimate the number of clusters within that radial range (on the assumption of an isotropic distribution). Our number densities are calculated within circular annuli, which should be appropriate if the true halo shape is roughly spherical.

Fig. 7 shows the projected GC number density as a function of radius for M31, with the correction for incomplete azimuthal coverage included. The data are presented in equally spaced logarithmic bins. The $\pm 1\sigma$ errors are determined assuming the number of GCs at a given radius is a Poisson process. Then in each bin, the upper (lower) end of the error bar is set to the value of underlying GC density for which the probability of observing a number of clusters as low (high) as we actually did, or lower (higher), is 15.87 per cent (Mulder 1983).

The profile shows a broken power-law behaviour. Inside a projected radius of $\sim$5 kpc, the radial number density profile of GCs is rather flat, as has been previously commented on in earlier studies (e.g. de Vaucouleurs & Buta 1978; Harris & Racine 1979; Wirth, Smarr & Bruno 1985; Battistini et al. 1993). While this behaviour could be genuine, it could also represent incompleteness in the samples at small radii. Indeed, detecting GCs against the high surface brightness bulge which dominates in this region remains a challenge even for modern day surveys. Beyond this inner region, the profile is much steeper out to a projected radius of $\sim$30 kpc after which it flattens again. This is the first time that this behaviour has been seen in M31 and is due to the fact that the new profile extends to radii of $\sim$100 kpc, more than three times further out than the earlier profiles of Racine (1991) and Battistini et al. (1993).
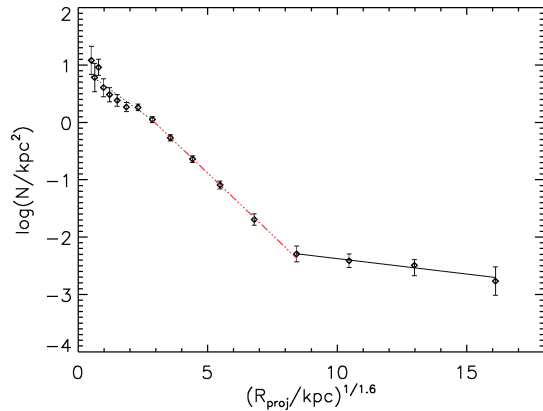
Figure 8. The radial profile of surface density of GCs in M31 against $R^{1/1.6}$, using the same bins as for Fig. 7. Linear fits have again been made to the inner, intermediate and outer regions as in Fig. 7. The flattening in the last three bins remains very clear.

A broken power-law fit is overlaid in Fig. 7 with best-fitting indices of -0.80 ± 0.10 inside of ~ 5 kpc, -2.88 ± 0.13 in the range $5 \lesssim R_{proj} \lesssim 30$ kpc and -0.87 ± 0.52 outside of ~ 30 kpc. Although this power-law representation is typically employed in extragalactic GC studies, it is clearly a rather poor description of the behaviour in M31, especially at intermediate radii, being too steep at small radii and too shallow at large radii in this range. Battistini et al. (1993) also noted that power-law fits were a poor representation of the radial number density profile of their sample of M31 GCs and investigated a number of other empirical fits. They found most success with an $R^{1/m}$ law, with $m \sim 1.6$. In Fig. 8, we show a profile of this form fitted to our current sample. Even though there have been many updates to the M31 GC catalogue since Battistini's work, this form still provides an excellent description of the radial number density profile over a significant radial range ($5 \lesssim R_{proj} \lesssim 30$ kpc). Indeed, this relation even provides a good fit for the outer halo GC profile, albeit with a different slope.

It is worth commenting that while the outer halo region is particularly rich in the more ECs (described below), these objects are not the primary cause of the flattening in the profile. Of the 36 GCs beyond the break in the GC surface density profile, only nine are ECs. This can be compared to two ECs from the 36 GCs in an annulus immediately interior to the break. If the radial surface density profile is constructed using only compact GCs, the break is still clearly present, but the slope at large radii is somewhat steeper.

4 THE EXTENDED CLUSTER POPULATION

One of the main results thus far from our GC search has been the discovery of a population of ECs within the halo of M31 (Paper I and Huxor et al. 2005). These objects typically have half-light radii of $\gtrsim 20$ pc and are significantly more extended than the normal GC population which has half-light radii of a few pc. Huxor et al. (2005) and Mackey et al. (2006) presented an analysis of the four brightest ECs discovered in the early stages of our survey. Here we present structural parameters for all 13 ECs in the sample studied here.

To investigate the structures of these clusters, we consider empirical King profiles,

$$\Sigma(r) = \Sigma_0 \left[\frac{1}{\left(1 + (r/R_c)^2\right)^{1/2}} - \frac{1}{\left(1 + (R_t/R_c)^2\right)^{1/2}} \right]^2 ,$$

where R_c and R_t are the core and tidal radii, respectively. These profiles were fitted to *V*-band photometry (in the case of the INT) or *g*-band (for MegaCam) photometry which were the shortest wavelength data available to us. King (1985) notes that the best cluster profiles are obtained by using the bluest images since statistical fluctuations due to individual red giants can be problematic at longer wavelengths. The fits were made to the cumulative flux measured within a series of apertures of increasing radii made with the IRAF/APPHOT photometry package.[6] Hence the fit, which minimized χ^2, was made to the integral of the King profile, which gives the total flux within a radius r:

$$C(r) = \Sigma_0 2\pi \left[\frac{R_c^2}{2} \ln(\alpha) - \frac{2R_c^2}{\beta} (\alpha)^{1/2} + \frac{r^2}{2\beta^2} + \frac{2R_c^2}{\beta} \right],$$

where

$$\alpha = 1 + (r/R_c)^2$$

and

$$\beta = \left(1 + (R_t/R_c)^2\right)^{1/2} .$$

There are some uncertainties associated with the values derived from our King profile fits. In the case of HEC7, contamination from foreground stars was removed first by using the 'patch' option in GAIA[7] to replace the affected region with an average of the background sky. Another cluster, HEC4, lies at the edge of a CCD chip, but the fractional area missing is small allowing us to still obtain photometry to a radius of 13 arcsec. Cluster HEC6 was so heavily affected by background galaxies that no profile fit could be attempted. In this case, a value for R_h was obtained by finding the aperture containing half the luminosity as given by our measurement of the total magnitude within a 12 arcsec aperture, and thus has a significant degree of uncertainty.

For four of the ECs studied, we can compare the ground-based profile fits made here with those derived from higher spatial resolution *Hubble Space Telescope* (*HST*)/ACS data and reported in Tanvir et al. (2011). The *HST* data allow for better removal of background galaxy contamination and give profile fits that are, for three of the four ECs, somewhat smaller than those found with the ground-based data. It is likely that this is mostly due to the limitations inherent in constructing profiles from ground-based data. This underscores the need to treat the quantities derived for faint ECs from ground-based fits with some caution.

It is of interest to compare the size distribution of ECs with that of the more compact GCs in M31. Although we would have liked to obtain profile fits for our entire sample of outer halo GCs, this proved to be impossible for the compact objects. The average seeing of our ground-based data was 1.2 arcsec, which corresponds to a physical size of ~ 4–5 pc at the distance of M31. Thus, we do not resolve classical GCs, which typically have core radii of 2–3 pc, to a sufficient extent to accurately fit their radial profiles. Instead, we use as a comparison sample the work by Barmby et al. (2007) and Tanvir et al. (2011) which presents King profile fits for compact M31 GCs from high-resolution imagery with *HST*. We also include the high-resolution ground-based imaging study of the outermost M31 halo GC by Mackey et al. (2010a). Fig. 9 shows

---

[6] IRAF is distributed by the National Optical Astronomy Observatories, which are operated by the Association of Universities for Research in Astronomy, Inc., under cooperative agreement with the National Science Foundation.
[7] GAIA, the 'Graphical Astronomy and Image Analysis' tool is now available as part of the Starlink Software Collection, via http://starlink.jach.hawaii.edu/
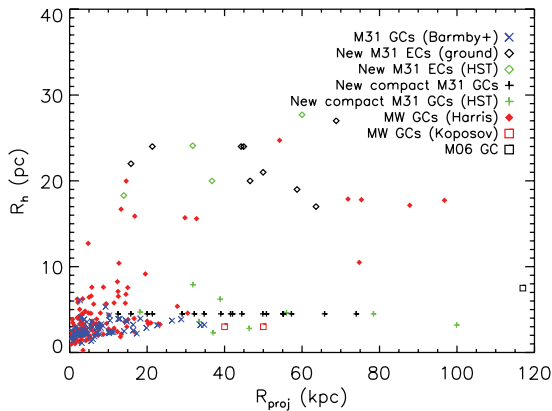
Figure 9. The distribution of R_h for M31 and MW GCs with projected galactocentric distance (kpc) showing the MW GCs (filled diamonds), new ECs from Paper I (open diamonds) and the Barmby et al. (2007) clusters that are in our catalogue (triangles). The new compact GCs from Paper I (plus signs) are shown with an R_h value of 4.5 pc (except for 10 clusters, where values are available from Tanvir et al. 2011). This is intended to show a maximum value, as they are unresolved in our data. See text for details.

the half-light radii (R_h) distribution of M31 ECs [black (green) open diamonds show ground-based (*HST*) measurements] and GCs (crosses) against projected galactocentric radius compared to the MW GCs (filled diamonds). We only show those members of the Barmby et al. (2007) sample that are also found in our master M31 GC catalogue described previously. Most of those in Barmby et al. (2007) that are not in our list are putative 'young clusters,' as indicated by the corresponding flag in the RBC data base. A further handful are not yet included in the RBC. Fig. 9 includes the newly found compact M31 GCs from Paper I (plus signs) which are plotted with an upper limit on the half-light radius of 4.5 pc. (black crosses), derived from the average seeing. The newly discovered GCs from Paper I with structural parameters derived from our *HST* data (Tanvir et al. 2011) are shown as green plus symbols. It can be seen that the M31 GCs exhibit a very different size distribution compared to those of the MW, in that the MW does not possess compact GCs at large galactocentric radii. There is also a suggestion of bimodality in the size distribution of M31 GCs at large radii with few GCs having R_h in the range from 8 to 15 pc.

The ECs are of particular interest since, as first noted by Huxor et al. (2005), they lie between classical GCs and dwarf spheroidal galaxies in a plot of M_V versus R_h (Fig. 10). The true nature of ECs – whether simply star clusters or dark matter dominated systems – remains unclear at present. Collins et al. (2009) present a measurement of the internal velocity dispersion in HEC12 (EC4) which was used to derive a mass-to-light ratio of $M/L = 6.7^{+15}_{-6.7}\,\mathrm{M_\odot/L_\odot}$. Although consistent with a globular star cluster, this result has large uncertainties and cannot be used to definitively exclude the presence of a modest amount of dark matter. The first three ECs reported in Huxor et al. (2005) were extreme in their large magnitudes and half-light radii. While these objects appeared to be somewhat isolated in the M_V–R_h plot, the additional clusters reported here indicate that ECs actually form a continuous, nearly vertical, sequence which overlaps at the faint end with the smaller, less luminous Palomar-type GCs found in the MW. Moreover, the new *HST* data suggest that the most extreme ECs are not as large as previously thought. However, they are still significantly more extended than typical GCs, and one might speculate whether a few of M31 ECs are higher luminosity analogues of some of the unusual
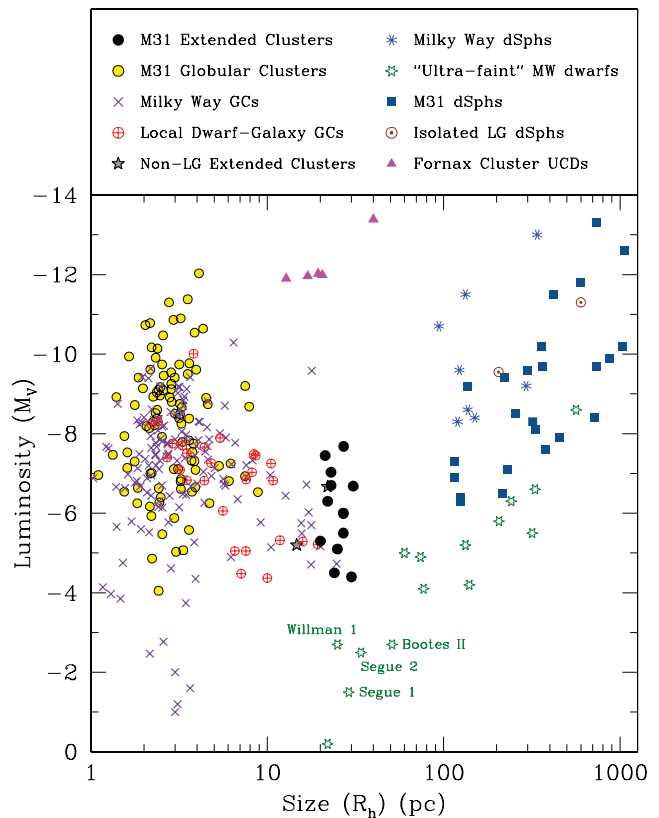

Figure 10. Plot of M_V against R_h of the ECs (filled circles) – with the data from Tanvir et al. (2011) used where available, shown with a range of low-mass stellar systems in the Local Group, including M31 GCs – circles (Barmby et al. 2007), MW GCs – crosses (Harris 1996; Koposov et al. 2007), GCs in Large Magellanic Cloud, Small Magellanic Cloud, Fornax and Sagittarius dwarf – crossed circles (Harris 1996; van den Bergh & Mackey 2004), the ECs found beyond the Local Group – filled stars (Da Costa et al. 2009; Mouhcine et al. 2010), ultra-compact dwarfs (UCDs) – triangles (Mieske, Hilker & Infante 2002; Drinkwater et al. 2003; De Propris et al. 2005), M31 dwarf galaxies – squares (Zucker et al. 2004, 2007; Harbeck et al. 2005; Martin et al. 2006; Ibata et al. 2007; Majewski et al. 2007; Irwin et al. 2008; McConnachie et al. 2008; Martin et al. 2009), classical MW dwarf galaxies – asterisks (Irwin & Hatzidimitriou 1995; McConnachie & Irwin 2006), the islolated Local Group dwarfs Cetus and Tucana – dotted circles (Saviane, Held & Piotto 1996; McConnachie & Irwin 2006) and the newly found low-luminosity MW dwarf galaxies – stars (Belokurov et al. 2008, 2010), for which the data of Martin, de Jong & Rix (2008) and de Jong et al. (2010) are used. Note that Segue 3 from Belokurov et al. (2010) has the structural parameters of a GC and so is plotted as a MW GC.

ultrafaint systems that have recently been discovered around the MW, such as Segue I (Belokurov et al. 2007). Some of the ultrafaints which most resemble ECs in terms of their luminosities and sizes are labelled in Fig. 10. There is still much debate about the true nature of the lowest luminosity ultrafaint systems, with opinions split between their (once?) being genuine dwarf galaxies as opposed to simple star clusters (e.g. Siegel, Shetrone & Irwin 2008; Niederste-Ostholt et al. 2009). In-depth imaging and spectroscopic studies of the M31 ECs as well as the ultrafaint galaxy population will provide further insight into this question.

5 DISCUSSION

We have presented a detailed study of the properties of the M31 GC system, with a particular focus on the halo region, using the largest

Table 1. Properties of the ECs. Columns (2)–(5) and (8)–(9) derived by fits to a King model. Columns (6) and (7) show values of R_c and R_h derived from recent *HST*/ACS imaging of HEC4, 5, 7 and 12, indicating errors in the ground-based data. The values for HEC6 are not derived from model fitting (see text for details). The cross identifications for the ECs in Huxor et al. (2005) and Tanvir (in preparation) are also given (H05 ID and T10 ID, respectively) where appropriate.

HEC ID	R_c (pc)	R_t (pc)	R_h (pc)	M_{V0} (model)	H05 ID	T10 ID	$R_c HST$ (pc)	$R_h HST$ (pc)	$M_{V0} HST$ (pc)
1	18	113	24	−6.0	–	–	–	–	–
2	12	83	17	−5.3	–	–	–	–	–
3	13	116	21	−4.5	–	–	–	–	–
4	16	140	26	−7.2	C3	EC3	25.9	18.3	−7.45
5	23	166	34	−7.3	C1	EC1	14.8	24.1	−7.68
6	–	–	24	−5.5	–	–	–	–	–
7	17	132	26	−7.8	C2	EC2	10.9	20.0	−7.03
8	11	58	22	−5.1	–	–	–	–	–
9	20	94	24	−6.0	–	–	–	–	–
10	10	135	19	−6.3	–	–	–	–	–
11	14	94	20	−6.7	–	–	–	–	–
12	32	84	27	−5.4	–	EC4	28.9	27.7	−6.68
13	23	114	27	−4.4	–	–	–	–	–

sample compiled to date of confirmed outer halo GCs. Wherever possible, we have compared the properties of the M31 halo GCs to those of their counterparts in the MW, often finding marked differences. In particular, M31 has far more GCs than the MW (at least by a factor of 3) and hosts a population of luminous compact GCs at large radius ($R_{proj} \lesssim 30$ kpc) that, aside from NGC 2419, is completely absent in the MW. M31's halo GC system is also considerably larger in physical extent than the MW's, with the most remote member currently known lying at a projected (3D) radius of 120 kpc (200 kpc)(Mackey et al. 2010a). It is unlikely that the difference in the outer halo GC populations is due to intrinsic differences in the shape of the GCLFs as we have shown that these are in good agreement, although the peak values in the two systems are slightly offset. The outer halo of the MW is inhabited primarily by Palomar-type GCs which are characterized by low luminosities and diffuse structures. Such clusters may also exist in the outer halo of M31 but, with typical $M_{V0} \gtrsim -5$, they are difficult to detect at that distance. A detailed assessment of the completeness of our M31 GC catalogue is required before we can determine whether M31 also possesses an excess of Palomar-type GCs at large radius and conduct a full analysis of the GCLF.

M31 hosts a population of luminous extended GCs which currently have no known counterparts in the MW. With $M_V \lesssim -6$ and $R_h \gtrsim 20$ pc, such objects should have been easily detected with the Sloan Digital Sky Survey (SDSS) out to a radius of ∼300 kpc within the Galactic halo (see fig. 10 in Koposov et al. 2008). It may be that similar objects exist in the MW halo yet are so few in number that they lie in parts of the sky not yet surveyed to sufficient depth. Alternatively, if ECs represent the tail of the size distribution of clusters at a given magnitude, then the absence of luminous examples in the MW may simply be due to the overall difference in the number of luminous GCs in the two systems. It is possible that some of the Palomar-type GCs in the MW are the low-luminosity analogues of the ECs seen in M31. It is of interest to note that many of the Palomar-type GCs have been shown to have younger ages than the bulk of the halo GCs and evidence supports the notion that many of these objects formed in dwarf galaxies that subsequently merged with the MW (e.g. Mackey & van den Bergh 2005). On the other hand, although EC4 does not appear to possess a dark matter halo, it cannot yet be ruled out that some ECs in M31 may share more of a kinship with dwarf galaxies – perhaps representing the bright tail of the population of ultrafaint dwarfs that has recently been uncovered in the MW (Belokurov et al. 2007). Some of the ECs are very faint and extended (e.g. HEC13, see Table 1), approaching Willman 1 in its properties.

The M31 GC population has often been considered to be somewhat redder than that of the MW, but with the reddenings we have adopted here the two systems have very similar colours. The halo GC populations ($R_{proj} \gtrsim 15$–30 kpc) in the two systems are especially noteworthy as they have almost identical $(V - I)_0$ colours which remain constant with radius. Using a subsample of M31 GCs with known [Fe/H] from CMD fitting, the mean metallicity of the outer halo GCs is [Fe/H] $\sim -1.9 \pm 0.2$ dex with no discernible gradient. This is in reasonable agreement with the mean for the outer MW GC population, [Fe/H] $\sim -1.7 \pm 0.2$ dex beyond 15 kpc, but considerably lower than the mean of the M31 stellar halo over the same radial range, [Fe/H] ~ -0.8 to -1.4 dex (Chapman et al. 2006; Kalirai et al. 2006; Koch et al. 2008; Richardson et al. 2009). This argues against the outer M31 field halo and halo GC system forming *in situ* at the same epoch. Furthermore, following the argument made by Searle & Zinn (1978) in the context of the MW, the lack of a metallicity gradient within the M31 halo GC population argues against the system having formed as part of a pressure-supported slow collapse. Instead, it is consistent with the picture wherein the outer GC system formed in a number of smaller subsystems which later merged to form the halo.

The large radial baseline spanned by our sample of GCs has enabled construction of the GC number density profile to hitherto unprobed distances. An unexpected result is the flattening of the profile beyond a radius of 30 kpc (see Figs 7 and 8). Intriguingly, a similar flattening has been observed in the surface brightness profile of the underlying stellar halo. This was first pointed out by Irwin et al. (2005) who used red giant branch (RGB) star count data in a large swath centred on the southern minor axis of M31 and later confirmed and extended by Ibata et al. (2007) who constructed an azimuthally averaged stellar surface brightness profile for the entire south-east quadrant of the galaxy, reaching distances of ∼150 kpc. Fig. 11 compares the M31 GC number density profile with the metal-poor minor axis profile of the stellar halo from Ibata et al. (2007). Both profiles flatten at roughly the same radius,
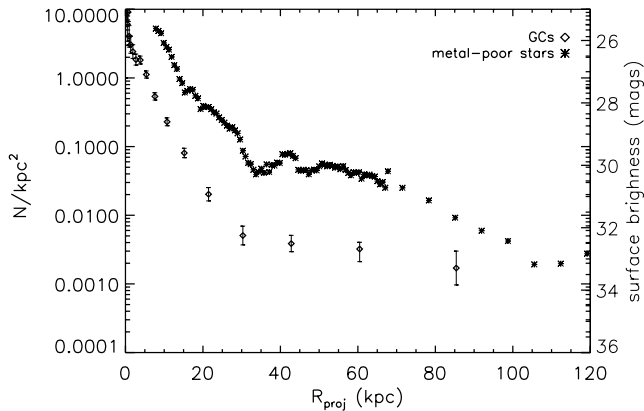
Figure 11. Plot of the M31 GC radial profile (diamonds) and the arbitrarily scaled minor axis metal-poor ($-3.0 <$ [Fe/H] < -0.7) profile (asterisks) from Ibata et al. (2007). Errors for the stellar profile are less than, or comparable to, the symbol size. The GC data are presented in the same bins as in Fig. 7. The flattening towards the central regions of M31 seen in that figure was more apparent than here as it employed a logarithmic axis for galactocentric radius.

~ 25–30 kpc; however, the GC number density profile appears flatter beyond this break than that of the field stars. Ibata et al. (2007) showed that, beyond a projected radius of 30 kpc, the stellar halo profile can be fitted with a power law of form $\Sigma_V \propto R^{-1.91\pm0.12}$, while we have found here that the GCs behave as $\propto R^{-0.87\pm0.52}$. It is unclear at present whether this difference should be viewed as significant. The slope of the stellar surface density profile is highly dependent on accurate subtraction of contaminating foreground stars, while the GC number density profile suffers from small number statistics at large radius.

The fact that both GC and field star populations reveal profile flattenings at around the same radius is consistent with the idea that accretion has played an important role in the formation of the outer halo. Abadi, Navarro & Steinmetz (2006) have used numerical simulations of galaxy formation within a Λ cold dark matter (ΛCDM) cosmological framework to investigate the structure of galaxies formed through a combination of *in situ* star formation and accretion. They show that beyond the luminous edge of the galaxy, defined as that radius at which the accreted stellar component starts to dominate over that of the *in situ* component, the slope of the radial surface brightness profile changes (see their fig. 4). Within this radius, which corresponds to 20 kpc in their simulations, the surface brightness profile is well fitted by a de Vaucouleurs bulge plus an exponential disc. At larger radii, the outer halo profile flattens significantly and can be fitted with a power law which varies from $\Sigma_V \propto R^{-2.3}$ at 30 kpc to $\propto R^{-2.9}$ at 100 kpc. This behaviour is qualitatively consistent with both the outer field star and GC number density profiles in M31; however, the observed radial fall-offs are shallower than the simulations predict (see also Ibata et al. 2007). It is intriguing that the GC number density profile in M31 has an outer slope that is reasonably close to that expected for the dark matter halo $-\propto R^{-1.5}$ – calculated over the range 25–100 kpc, using the parameters given in Klypin, Zhao & Somerville (2002).

The lack of a metallicity gradient in the halo GC population and the shape of the GC areal number density profile both provide support for accretion playing a significant role in building up the M31 GC system. The sheer number of outer halo GCs and the existence of particularly extended clusters could also be signatures of this mode of formation. In this scenario, the overall differences in the halo GC populations of the MW and M31 could be the result of the two galaxies having experienced a different number of accretion events, or accretions of a different type. For example, the MW may have accreted mostly low-mass satellites which carry few, if any, associated GCs, while M31 may have undergone at least one more substantial merger (e.g. Fardal et al. 2008).

While ample evidence exists for satellite accretion events contributing field stars to stellar haloes (Ibata, Gilmore & Irwin 1994; Ibata et al. 2001; Ferguson et al. 2002; McConnachie et al. 2009), direct evidence for GC systems being built up in this manner has been less forthcoming. One notable example is the Sagittarius dwarf that is currently being accreted on to the MW and which has been shown to be contributing at least one massive compact GC (M54) as well as several Palomar-type clusters (Da Costa & Armandroff 1995; Bellazzini, Ferraro & Ibata 2003; Forbes & Bridges 2010). More recently, direct evidence for GC accretion in M31 has been presented by Mackey et al. (2010b). These authors examine the spatial correlation between the positions of a sample of halo GCs (many of which are included in the present sample) and underlying tidal debris streams. They use a Monte Carlo approach to show that the probability of the observed degree of alignment being due to chance is low, below 1 per cent, and conclude that the observed spatial coincidence reflects a genuine physical association. They further argue that the accretion of cluster-bearing satellite galaxies could plausibly account for $\gtrsim 80$ per cent of the M31 GC population beyond 30 kpc. The properties of the M31 halo GC population presented in this paper are wholly consistent with this idea.

Finally, it is interesting to compare the halo GC system of M31, the most populous and extended GC system of a disc galaxy in the local Universe, with that of the well-studied giant elliptical M87. Wide-field ground-based studies of M87's GC population have recently been carried out by Tamura et al. (2006a,b) and Harris (2009), enabling the system to be traced out to distances of $\gtrsim 100$ kpc. Since GCs at the distance of M87 (~ 16 Mpc) are unresolved from the ground, these studies need to rely on statistical subtraction to detect and characterize the GC population which can lead to some uncertainties, particularly at large radii. Both Harris (2009) and Tamura et al. (2006a) find that the red GCs in M87 are concentrated in the central regions of the galaxy ($\lesssim 50$ kpc), while the blue population can be traced out to at least 100 kpc and shows no evidence for a colour gradient in these parts. This is very similar to our finding of a large colour spread in the inner regions of M31 with a very uniform blue population dominating in the outer halo. The M87 studies also derive radial number density profiles for the GCs and show a single-profile form (either $R^{1/4}$ or power-law R^{-n}, where n smoothly increases with radius) fits the data well out to $\gtrsim 150$ kpc. However, the profile shape at large radius is highly dependent on the assumed level of contaminating sources (e.g. foreground stars, compact background galaxies), and it is not yet possible to place rigorous constraints on the form of M87's GC distribution in these parts (although the GC system of M87 has the benefit of not suffering from problems associated with small number statistics). Indeed, inspection of fig. 5 from Tamura et al. (2006a) hints at a possible flattening in the number density profile at ~ 90 kpc, similar to what we see at ~ 30 kpc in M31. Tamura et al. (2006a) also note that the blue GCs in M87 are more extended than the stellar light, but recent work by Janowiecki et al. (2010) and Williams et al. (2007) shows M87's stellar halo is far larger than previously thought. Using very deep wide-field imagery, they trace the M87 surface brightness profile to ~ 180 kpc at which point the V-band surface brightness falls below their detection limit of 29 mag arcsec^{-2}. This is entirely consistent with the extent of the blue GC population. In summary, although

M87 and M31 differ vastly in terms of their inner morphologies and galaxy environments, their halo GC populations show some striking similarities. Perhaps the properties of halo GC systems are determined by processes which are largely decoupled from those which shape the main components of galaxies as we see them today.

6 SUMMARY

We have investigated the global properties of the M31 GC system using an updated sample which includes newly discovered GCs reported by us in Paper I as well as other revisions to the RBC. We also derive structural parameters for 13 ECs. We find that many of these are less luminous and less extended than those presented in Huxor et al. (2005), bridging a gap between them and the 'Palomar-type' GCs found in the MW.

Mackey et al. (2010b) recently showed that many clusters in the outer regions of M31 are physically associated with tidal streams, and the results presented in this paper are entirely consistent with this scenario. Specifically, we find no evidence for a significant radial colour/metallicity gradient at large galactocentric radii, as expected from accretion. We also find evidence for a flattening in the GC number density radial profile in M31 occurring at a projected radius of ~30 kpc, coinciding with a similar feature in the underlying stellar halo component. Abadi et al. (2006) have shown that such a flattening occurs naturally in galaxies that grow through a combination of *in situ* star formation and accretion, with the point of transition indicating the radius beyond which the bulk of the matter has been accreted.

Wherever possible, we have compared the properties of the M31 halo GC system to that of the MW, often finding marked differences. Although the overall form of the luminosity functions is similar in both systems down to $M_{V0} \approx -5$, M31 possesses a significant population of luminous and compact GCs at large galactocentric radii which, aside from NGC 2419, have no counterpart in the MW. M31 also has a number of extended GCs, many of which are far larger than those in the MW (Fig. 10). On the other hand, halo GCs in M31 and the MW have similarly blue mean colours beyond $R_{proj} > 15$–30 kpc, with little dispersion, indicating that old metal-poor populations dominate in both cases. We suggest that the differences between the two GC systems could be, at least partly, explained by the differing accretion histories that M31 and MW have experienced.

Finally, our work illustrates the importance of extending study of GC systems to large galactocentric radii. The accretion of cluster-bearing satellites is likely the dominant process in building up the halo GC populations of galaxies, while *in situ* formation may contribute the most to the populations at smaller radii. As a result, it is the halo GC populations that have the most to tell us about the hierarchical assembly of galaxies. Large-area surveys with telescopes such as Pan-STARRS and Large Synoptic Survey Telescope (LSST) should contribute significantly to building samples of GC candidates in the remote outskirts of galaxies within and beyond the Local Group, while spectroscopic campaigns will become increasingly necessary to weed out contaminants in these sparsely populated parts.

REFERENCES

Abadi M. G., Navarro J. F., Steinmetz M., 2006, MNRAS, 365, 747
Alves-Brito A., Forbes D. A., Mendel J. T., Hau G. K. T., Murphy M. T., 2009, MNRAS, 395, L34
Barmby P., Huchra J. P., Brodie J. P., Forbes D. A., Schroder L. L., Grillmair C. J., 2000, AJ, 119, 727
Barmby P., McLaughlin D. E., Harris W. E., Harris G. L. H., Forbes D. A., 2007, AJ, 133, 2764
Battistini P. L., Bonoli F., Casavecchia M., Ciotti L., Federici L., Fusi-Pecci F., 1993, A&A, 272, 77
Bellazzini M., Ferraro F. R., Ibata R., 2003, AJ, 125, 188
Belokurov V. et al., 2007, ApJ, 654, 897
Belokurov V. et al., 2008, ApJ, 686, L83
Belokurov V. et al., 2010, ApJ, 712, L103
Brodie J. P., Strader J., 2006, ARA&A, 44, 193
Caldwell N., Harding P., Morrison H., Rose J. A., Schiavon R., Kriessler J., 2009, AJ, 137, 94
Chapman S. C., Ibata R., Lewis G. F., Ferguson A. M. N., Irwin M., McConnachie A., Tanvir N., 2006, ApJ, 653, 255
Collins M. L. M. et al., 2009, MNRAS, 396, 1619
Crampton D., Cowley A. P., Schade D., Chayer P., 1985, ApJ, 288, 494
Da Costa G. S., Armandroff T. E., 1995, AJ, 109, 253
Da Costa G. S., Grebel E. K., Jerjen H., Rejkuba M., Sharina M. E., 2009, AJ, 137, 436
de Jong J. T. A., Martin N. F., Rix H.-W., Smith K. W., Jin S., Macciò A. V., 2010, ApJ, 710, 1664
De Lucia G., Helmi A., 2008, MNRAS, 391, 14
De Propris R., Phillipps S., Drinkwater M. J., Gregg M. D., Jones J. B., Evstigneeva E., Bekki K., 2005, ApJ, 623, L105
de Vaucouleurs G., Buta R., 1978, AJ, 83, 1383
Drinkwater M. J., Gregg M. D., Hilker M., Bekki K., Couch W. J., Ferguson H. C., Jones J. B., Phillipps S., 2003, Nat, 423, 519
Eggen O. J., Lynden-Bell D., Sandage A. R., 1962, ApJ, 136, 748
Elson R. A., Walterbos R. A. M., 1988, ApJ, 333, 594
Fan Z., Ma J., de Grijs R., Yang Y., Zhou X., 2006, MNRAS, 371, 1648
Fan Z., Ma J., de Grijs R., Zhou X., 2008, MNRAS, 385, 1973
Fan Z., de Grijs R., Zhou X., 2010, ApJ, 725, 200
Fardal M. A., Babul A., Guhathakurta P., Gilbert K. M., Dodge C., 2008, ApJ, 682, L33
Ferguson A. M. N., Irwin M. J., Ibata R. A., Lewis G. F., Tanvir N. R., 2002, AJ, 124, 1452
Font A. S., Johnston K. V., Ferguson A. M. N., Bullock J. S., Robertson B. E., Tumlinson J., Guhathakurta P., 2008, ApJ, 673, 215
Forbes D. A., Bridges T., 2010, MNRAS, 404, 120
Fusi Pecci F., Bellazzini M., Buzzoni A., De Simone E., Federici L., Galleti S., 2005, AJ, 130, 554
Galleti S., Federici L., Bellazzini M., Fusi Pecci F., Macrina S., 2004, A&A, 416, 917
Galleti S., Federici L., Bellazzini M., Buzzoni A., Fusi Pecci F., 2006, A&A, 456, 985

Galleti S., Bellazzini M., Federici L., Buzzoni A., Fusi Pecci F., 2007, A&A, 471, 127

Harbeck D., Gallagher J. S., Grebel E. K., Koch A., Zucker D. B., 2005, ApJ, 623, 159

Harris W. E., 1996, AJ, 112, 1487

Harris W. E., 2009, ApJ, 703, 939

Harris W. E., Racine R., 1979, ARA&A, 17, 241

Huchra J. P., Brodie J. P., Kent S. M., 1991, ApJ, 370, 495

Huxor A. P., Tanvir N. R., Irwin M. J., Ibata R., Collett J. L., Ferguson A. M. N., Bridges T., Lewis G. F., 2005, MNRAS, 360, 1007

Huxor A. P., Tanvir N. R., Ferguson A. M. N., Irwin M. J., Ibata R., Bridges T., Lewis G. F., 2008, MNRAS, 385, 1989 (Paper I)

Huxor A., Ferguson A. M. N., Barker M. K., Tanvir N. R., Irwin M. J., Chapman S. C., Ibata R., Lewis G., 2009, ApJ, 698, L77

Ibata R. A., Gilmore G., Irwin M. J., 1994, Nat, 370, 194

Ibata R., Irwin M., Lewis G., Ferguson A. M. N., Tanvir N., 2001, Nat, 412, 49

Ibata R., Martin N. F., Irwin M., Chapman S., Ferguson A. M. N., Lewis G. F., McConnachie A. W., 2007, ApJ, 671, 1591

Irwin M., Hatzidimitriou D., 1995, MNRAS, 277, 1354

Irwin M. J., Ferguson A. M. N., Ibata R. A., Lewis G. F., Tanvir N. R., 2005, ApJ, 628, L105

Irwin M. J., Ferguson A. M. N., Huxor A. P., Tanvir N. R., Ibata R. A., Lewis G. F., 2008, ApJ, 676, L17

Janowiecki S., Mihos J. C., Harding P., Feldmeier J. J., Rudick C., Morrison H., 2010, ApJ, 715, 972

Kalirai J. S. et al., 2006, ApJ, 648, 389

Kim S. C. et al., 2007, AJ, 134, 706

King I. R., 1985, in Hut P., Goodman J. J., eds, Proc. IAU Symp. 113, Dynamics of Star Clusters. Reidel, Dordrecht, p. 1

Klypin A., Zhao H., Somerville R. S., 2002, ApJ, 573, 597

Kobulnicky H. A. et al., 2005, AJ, 129, 239

Koch A. et al., 2008, ApJ, 689, 958

Koposov S. et al., 2007, ApJ, 669, 337

Koposov S. et al., 2008, ApJ, 686, 279

Kurtev R., Ivanov V. D., Borissova J., Ortolani S., 2008, A&A, 489, 583

McConnachie A. W., Irwin M. J., 2006, MNRAS, 365, 1263

McConnachie A. W., Irwin M. J., Ferguson A. M. N., Ibata R. A., Lewis G. F., Tanvir N., 2005, MNRAS, 356, 979

McConnachie A. W. et al., 2008, ApJ, 688, 1009

McConnachie A. W. et al., 2009, Nat, 461, 66

Mackey A. D., van den Bergh S., 2005, MNRAS, 360, 631

Mackey A. D. et al., 2006, ApJ, 653, L105

Mackey A. D. et al., 2007, ApJ, 655, L85

Mackey A. D. et al., 2010a, MNRAS, 401, 533

Mackey A. D. et al., 2010b, ApJ, 717, L11

Majewski S. R. et al., 2007, ApJ, 670, L9

Martin N. F., Ibata R. A., Irwin M. J., Chapman S., Lewis G. F., Ferguson A. M. N., Tanvir N., McConnachie A. W., 2006, MNRAS, 371, 1983

Martin N. F., de Jong J. T. A., Rix H.-W., 2008, ApJ, 684, 1075

Martin N. F. et al., 2009, ApJ, 705, 758

Mieske S., Hilker M., Infante L., 2002, A&A, 383, 823

Mouhcine M., Harris W. E., Ibata R., Rejkuba M., 2010, MNRAS, 404, 115

Mulder P. G. H., 1983, Am. J. Epidemiology, 117, 377

Niederste-Ostholt M., Belokurov V., Evans N. W., Gilmore G., Wyse R. F. G., Norris J. E., 2009, MNRAS, 398, 1771

Peacock M. B., Maccarone T. J., Knigge C., Kundu A., Waters C. Z., Zepf S. E., Zurek D. R., 2010, MNRAS, 402, 803

Perrett K. M., Bridges T. J., Hanes D. A., Irwin M. J., Brodie J. P., Carter D., Huchra J. P., Watson F. G., 2002, AJ, 123, 2490

Racine R., 1991, AJ, 101, 865

Richardson J. C. et al., 2009, MNRAS, 396, 1842

Saviane I., Held E. V., Piotto G., 1996, A&A, 315, 40

Schlegel D. J., Finkbeiner D. P., Davis M., 1998, ApJ, 500, 525

Searle L., Zinn R., 1978, ApJ, 225, 357

Sharov A. S., 1988, Soviet Astron. Lett., 14, 33

Siegel M. H., Shetrone M. D., Irwin M., 2008, AJ, 135, 2084

Tamura N., Sharples R. M., Arimoto N., Onodera M., Ohta K., Yamada Y., 2006a, MNRAS, 373, 588

Tamura N., Sharples R. M., Arimoto N., Onodera M., Ohta K., Yamada Y., 2006b, MNRAS, 373, 601

van den Bergh S., Mackey A. D., 2004, MNRAS, 354, 713

West M. J., Côté P., Marzke R. O., Jordán A., 2004, Nat, 427, 31

White S. D. M., Frenk C. S., 1991, ApJ, 379, 52

Williams B. F. et al., 2007, ApJ, 654, 835

Wirth A., Smarr L. L., Bruno T. L., 1985, ApJ, 290, 140

Zepf S. E., Ashman K. M., 1993, MNRAS, 264, 611

Zucker D. B. et al., 2004, ApJ, 612, L121

Zucker D. B. et al., 2007, ApJ, 659, L21

This paper has been typeset from a T_EX/L^AT_EX file prepared by the author.